A practical underwater 3D-Laserscanner

Marc Hildebrandt*, Jochen Kerdels*, Jan Albiez* and Frank Kirchner*
*Underwater Robotics Department
DFKI Bremen
Germany, 28359 Bremen
Email: marc.hildebrandt@dfki.de

***Abstract*— A number of attempts have been made to use the benefits of 3D-Laserscanning techniques in the underwater environment. Unfortunately, due to a number of operative problems with such devices, their accuracy and therefore applicability remains quite low. This paper specifically focuses on these practical issues by expanding on previous works in this area and improving their usability. The result is a calibration procedure for triangulation-based 3D-laserscanners for the underwater environment which provides a very promising precision and reliability, but at the same time does not demand exaggerated deployment overhead.**

I. Introduction

The problems with existing 3D-laserscanners for the underwater environment can be categorized into the areas of system concept and calibration issues. Problems in both areas will be addressed.

The term 3D-laserscanner is used for two different systems: LIDAR-scanners and triangulation-based scanners. In a LIDAR-system the time TOF (time of flight) of the laser beam is measured, resulting in a depth measurement[4] (see figure 1). The laser is fired in pulsed-mode, each pulse yielding one distance measurement. To achieve multi-dimensional mapping the laser beam is moved over the object using a 1D or 2D-scanning head, resulting in a 2D or 3D image of the object. Unfortunately construction of this type of 3D-laserscanner requires very sensitive equipment, so usually systems have to be bought. A number of commercially available LIDAR-scanners with different applications are listed in [7]. They usually utilize lasers in the range of 650-1500nm, since this laser technology is best understood and cheap. Typical scanning frequencies for this type of scanner are in the range of 250-500.000 points per second, while there usually is a decrease in angular- and distance-precision when operating at peak frequencies. Besides maximum scanning ranges (15-1.500 meters) these systems also have minimum scanning distance, usually in the range of 0.1-0.5 meters. Beam energies range from 0.5 to 23mW. Triangulation-systems measure the displacement of the laser beam in the camera image, resulting from a nonzero distance (called baseline) between the laser source an the camera. This distance can be translated into a depth information. Triangulation-systems usually utilize a line laser source with a 1D-scanning head [5] (see figure 2), resulting in a 3D image of the scanned scene. Scanning speeds and accuracies vary greatly, depending on a number of factors described in section II.

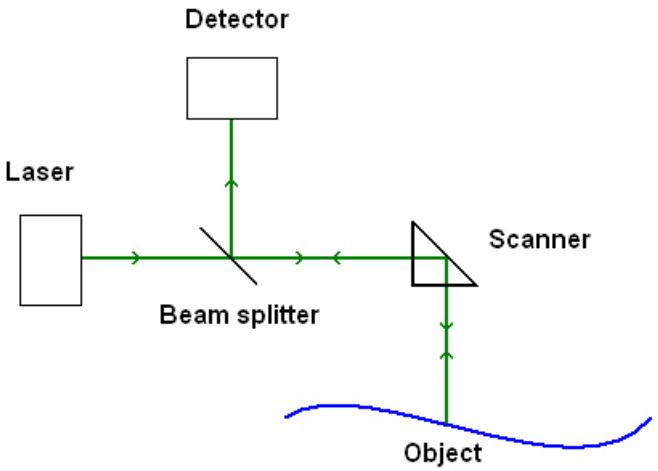

Fig. 1. LIDAR-type system using the TOF (time of flight) to obtain depth information.

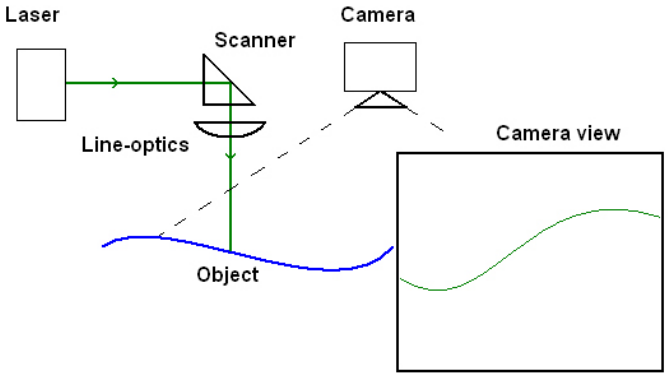

Fig. 2. Triangulation-type system using distortion of the laser line in the camera image as depth information.

Common for both types of 3D-laserscanner are the following basic components:

- Laser source
- Scanning head
- Detector

For underwater deployment a watertight housing has to be added. This component has considerable effect on the performance of the system, since losses and beam-path deviations at the air-glass-water-interface are significant. Both flat and

domed interfaces have been used in 3D-laserscanner systems ([1],[10]), both dealing with their respective advantages and disadvantages. Especially for the triangulation based scanners it has to be decided, if camera and laser source share a common housing or are sealed separately.

A critical component in both types of laserscanner is the laser source. Typical industry-used laser wavelengths lay in the range of 650-1500nm, for which the absorption coefficients are too high (0.0047-21.59cm^{-1}) [8], resulting in effective scanning ranges of well below one meter for the 650nm sources and mere millimeters for the 1500nm sources. The ideal absorption wavelength for clear water lies around 420nm (absorption coefficient 0.000062cm^{-1}) [9], in the blue spectrum. Unfortunately lasers in this wavelength are still very expensive, rather bulky and not very energy-efficient. The green spectrum around 532nm is much more common, and its similar absorption coefficient of 0.000498cm^{-1} [9], only one order of magnitude higher currently makes the choice of a green laser the cost-benefit ideal. Beam geometry is another important aspect, since divergence, beam uniformity and beam diameter directly impact scanning accuracy. Divergence dictates the growth of the laser spot in respect to distance, so the resolution decreases with increasing scanning range. Beam uniformity especially is a problem with triangulation-type laserscanners including a line optics, which usually produces a Gaussian intensity distribution and induces optical disturbances due to impurities of the lenses (see figure 3). To avoid these effects special non-Gaussian laser line optics can be used, at the expense of size and monetary cost. Beam width (or line width for triangulation-type systems) is a critical factor, since smaller values offer better resolution, but require more sensitive detectors.

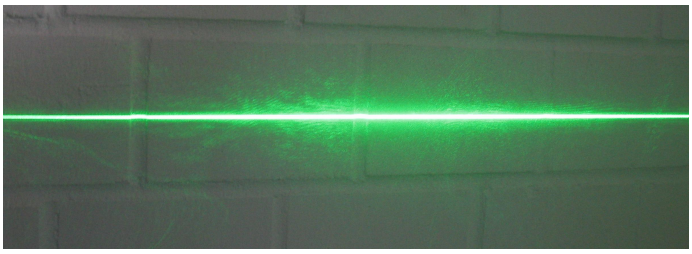

Fig. 3. Non-uniform laser line with disturbances produced by simple line optics.

The scanning head should allow the 2D/1D movement of the laser beam/line. Different approaches have been used as actuators for the mirror, but all have in common that they have to be optimized for size, speed and precision. The angular accuracy of scanning heads lies in the order of 0.01 deg for integrated industrial systems ([7]), less sophisticated systems utilizing servomotors reach orders of 0.1 deg.

The detector greatly differs between the two systems: for LIDAR-type systems a photodiode is used, which measures the time of arrival of the previously emitted beam. Avalanche-type photodiodes, which offer a very good sensitivity at the price of SNR (signal-noise-ratio) are usually used. The amplitude of the received signal can be interpreted as the reflectivity of the sampled surface. Systems including this value in their output are called imaging laserscanners, since an interpretation of the reflectivity as 8bit greyscale value yields an greyscale-photograph like image of the scene (see e.g. [11]). For triangulation-type systems the detector is a 2D imaging sensor. Additional to the sensitivity the horizontal and vertical resolution as well as the FOV (field of view) are of importance, since they impact scanning resolution and obviously the laserscanner can only work for objects inside the cameras FOV. Greyscale cameras usually have better sensitivity, since they do not incorporate IR and colour filters. A higher vertical camera resolution improves the scanner resolution up to the point in which the projected laser line occupies more than a pixel in the image, at which point the width of the laser line has to be decreased to improve resolution. Increased horizontal resolution increases the computational complexity of the system. It is obvious that the FOV of the camera and the fan angle of the laser line optics should be selected equal. Depending on the type of surface the laser is reflected from, the high beam intensity may over-saturate the camera. CCD cameras are by concept much more sensitive to this type of oversaturation than CMOS cameras.

Most LIDAR-systems cannot be utilized in the underwater environment since they use laser wavelengths in the 650-1500nm range, which makes them unsuitable for the underwater environment by design. One of the few available 532nm-LIDAR-scanners is described in [6], but no references of its usage in the underwater environment could be found up to date, which is considered to be a result of its size, power requirements and high monetary cost.

A key advantage of triangulation-systems is the fact, that most underwater vehicles already incorporate a camera. This opens the possibility to upgrade an existing system by simply adding the laser source and the scanning head in a separate housing. Since virtually all above-mini ROV systems use an open-frame concept, mounting of this additional component should pose no difficulty.

This paper will focus on the calibration of a triangulation-type laserscanner. Common problems of this procedure will be addressed and a novel procedure addressing most of these points will be presented in section II. The experimental results with this new calibration method will then be shown in section III and finally a conclusion and an outlook to future work will be given in section IV.

II. Calibration

The calibration procedure has the aim to find the geometrical parameters of the laserscanning system. Figure 4 shows the schematic overview of the laserscanner system. The geometrically defining parameters of the system are the baseline b, e.g. the vertical distance between the optical axis of the camera and the origin of the scanning head, the pitch angle of the camera α and the minimum, maximum and mean angles of the scanning head (with the mean angle denoted β) moving the laser line. Acquisition of these parameters

was often simplified by previous works, where the origin of these values is not explicitly explained, so it is assumed that they are measured manually (see e.g. [1], [3]). This method is highly questionable due to a number of reasons: The achievable accuracy of manually measuring these values is relatively low. Manually measuring the baseline distance means exact knowledge of the camera's optical axis position inside the watertight housing, which is impractical. A similar problem applies to the measurement of the camera's pitch angle, aggravated by the general inaccuracy of angular measurement. Measurement of the minimum, maximum and even the intermediate angles of the scanning head is comparatively easy, as a planar object can be placed in the baseline-optical-axis-plane, the laser line's projection onto it can be marked and the respective angle measured. Still this is not very accurate. These problems could be addressed by modelling these uncertainties into the geometrical laserscanner model, but a different approach will be investigated in this paper. Other calibration procedures address this problem, but require sophisticated bulky devices for calibration (e.g. [2]) which are impractical for most practical situations.

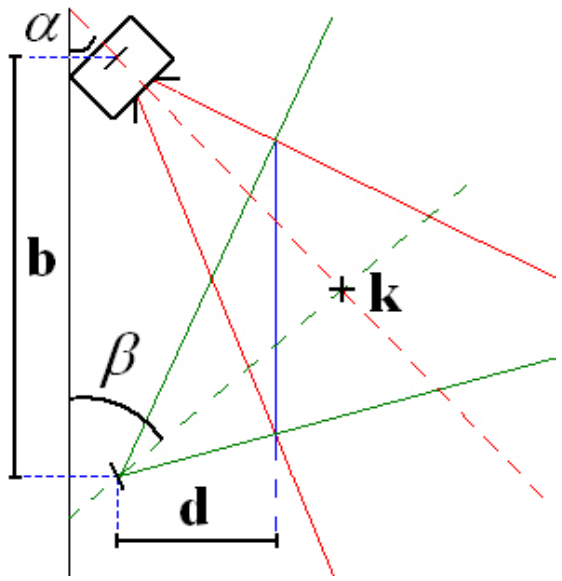

Fig. 4. Schematic of the laserscanner system with all modelled variables: The baseline b, angle between the baseline and the optical camera axis α, the middle scanning position of the scanning head β, the ideal scanning distance d and the laser-optical axis intersection point k.

The calibration procedure has the following steps:

- Intrinsic camera calibration
- For each scanning head position
  - For two different arbitrary calibration rig positions
    - Computation of the pose of a calibration rig
    - Determination of the laser line position in the camera image (on the calibration rig)
    - Description of the laser line as line in $\mathbb{R}^3$ in the camera's coordinate system
  - Computation of the plane described by the two lines acquired for each scanner position
- Intersection of all planes, forming a line in $\mathbb{R}^3$ intersecting the scanning head's position
- Calculation of the baseline length by determination of the distance between this line and the camera position (origin)
- Computation of the scanning head angle β by intersection of the laser plane with the baseline plane
- Positioning the calibration rig in such a way, that the laser line appears exactly at the centre of the image
- Computation of the camera pitch angle α from the resulting trigonometric relations

The advantages of this procedure are obvious: Besides the calibration rig no other external devices are necessary and the calibration rig is a simple planar object with a printed-on pattern. There is no need to move the rig in a pre-defined fashion, the only constraints being that it has to stay in the image and the laser line has to be visible on it. This makes it well suitable for in-the-field- as well as underwater application.

Intrinsic camera calibration is done using Zhang's algorithm [12]. It yields the necessary intrinsic camera parameters after a chessboard-type calibration rig is moved to different positions in front of the camera, and is widely used because of its simplicity and performance. Computation of the pose of the calibration rig in the second step is done by Zhang's algorithm for extrinsic calibration: using the same chessboard calibration rig it yields the pose of the chessboard on the calibration rig in the camera coordinate system. Since the calibration rig is a planar surface, this information can be used to obtain the plane $\mathrm{R} : \mathbf{n} \cdot \mathbf{X} + d = 0$ with the plane normal $\mathbf{n}$ and the distance of the plane from the origin d derived from the calibration rig pose. Using the dual-field calibration rig depicted in figure 5 the area in which the laser line is expected can now be determined. After detection of the laser line on the calibration rig its equation is stored as $\mathrm{L}_i^n(\lambda) = \mathbf{r}_i^n + \lambda\,(\mathbf{l}_i^n - \mathbf{r}_i^n)$, with i being the scanning head angle, n the running index for the two consecutive scans and $\mathbf{l}_i^n$ and $\mathbf{r}_i^n$ being two points on the line. After both scans the two lines are combined to form the laser projecting plane $\mathrm{P}_i : \mathbf{o}_i \cdot \mathbf{X} + m_i = 0$ with $\mathbf{o}_i = (\mathbf{r}_i^0 - \mathbf{l}_i^0) \times (\mathbf{r}_i^0 - \mathbf{l}_i^1)$ the normal of the plane, and $m = \left|\mathbf{r}_i^0\right|$ the distance from origin. Computing the intersection of all these planes should in theory yield a single line. Mathematically the intersection of two planes would suffice, but increasing the number of planes will lead to more robust results. Further another information can be obtained from this: consecutively intersecting the planes P_i and P_{i+1} results in $i-1$ lines. Due to imperfections in the optics and the air/glass/water-interface there is a virtual baseline for each scanning head position (see [1]). This change in the baseline-length b is directly visible in the acquired data and can be used to improve the accuracy of the laserscanning system. The angle β_i is the angle between each laser plane P_i and the baseline plane $\mathrm{B} : \begin{pmatrix} 1 \\ 0 \\ 0 \end{pmatrix} \cdot \mathbf{X} = 0$. Due to the projective nature of the laser fan the baseline plane can be simplified in this manner without harming the resulting

angle.

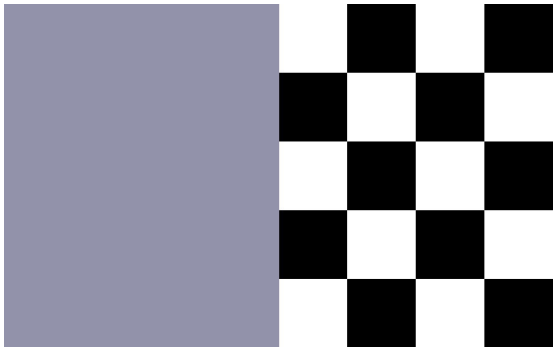

Fig. 5. The used calibration rig, with the chessboard-pattern on the right for pose estimation, and a good-contrast area on the left for laser line detection.

In order to compute the camera pitch angle α a last calibration step has to be made: the calibration rig has to be placed in such a manner, that the laser line is visible at the exact centre of the image. The image centre is one of the intrinsic parameters aquired by intrinsic camera calibration. This results in the definition of the point k (see figure 4), which makes the computation of α a matter of simple trigonometric relations, since the distance between k and the origin is known (it is the z-coordinate of the calibration rig at that frame, since its position is measured in the camera coordinate system) the law of sines can easily be applied: $\alpha = \pi - \beta - \left(\sin^{-1}\left(\frac{b\sin(\beta)}{k_z}\right)\right)$.

III. Experimental Results

The experimental system consist of a 20mW, 532nm line-laser with a horizontal FOV of 90 deg. It is mounted onto a servomotor and can be rotated 45 deg with an accuracy of 0.15 deg. It feature a circular housing made of Perspex which reduce the deviation at the air/glass/water interface. Due to mechanical constraints the laser source could not be mounted at the centre of the housing, so there is a small beam deviation introduced. The camera uses a 640x480 b/w CMOS sensor which is able to provide up to 200 FPS at full resolution. It has an Ethernet interface, yielding high quality images. The lens has a FOV of 90 deg and excellent depth of field, allowing good focus for different object distances. The camera housing features a planar borosilicate glass window. Both housings are fitted to a frame, the camera atop of the scanner housing (see figure 6). Tilt of the camera and the scanner housing can be easily varied, as well as their distance. The mounting distance however is not necessarily the same as the baseline, since the position of the CMOS-sensor inside the camera housing can only be estimated, and does not lie on the mounting plane. Theoretically this system should be able to yield a full 3D-scan consisting of 307200 3D-points in 2.4 seconds. This value simply derives from the time it takes the camera to acquire 480 images while the laser is swept across the image from its maximum to minimum value. The theoretical value of 307200 scan points will not be achieved in practice, since it only applies for objects at the ideal scanning distance d.

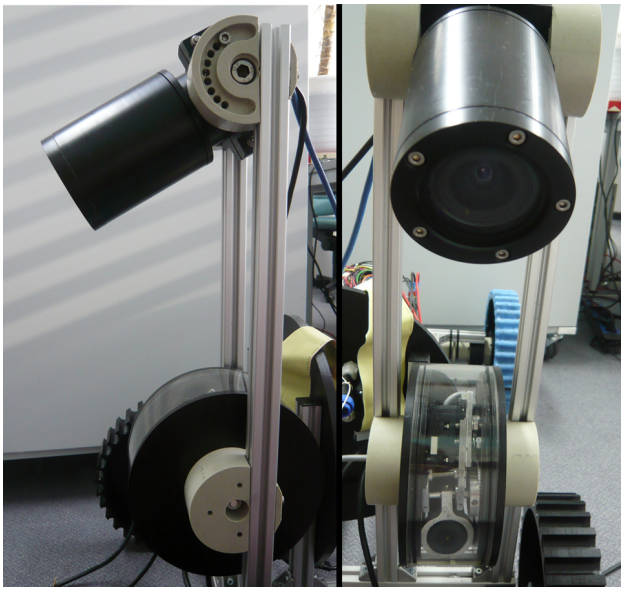

Fig. 6. The experimental system mounted onto an underwater crawler.

One of the experiments conducted was to determine the quality of 3D-pose estimation of the calibration rig. To this end the calibration rig was moved along pre-defined paths using an industrial robot (Mitsubushi PA10). The resulting trajectory data can be seen in figure 7.

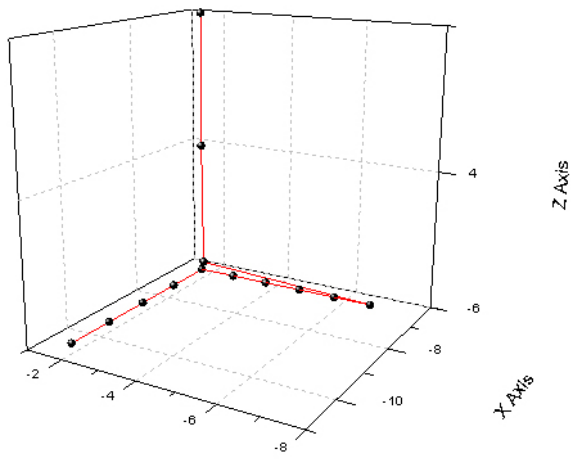

Fig. 7. Positions of the calibration rig as recorded from the industrial robot moving it.

This trajectory is observed by the laserscanner camera, and the pose estimation results are shown in figure 8. The two plots cannot be directly compared since they base on different coordinate systems (the first using the robot's centre als origin, the second the camera's origin), but it can clearly be seen, that they form the same pattern, and the angles at the intersection of the three lines are nearly 90 degrees.

After confirmation of the suitability of the pose estimation, the calibration procedure was tested. As reference a set of system parameters was manually measured prior to the

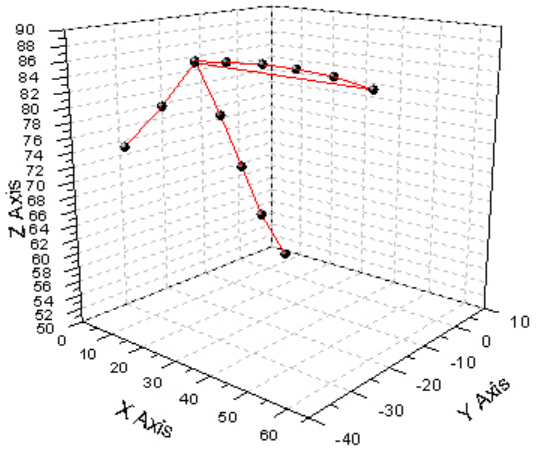

Fig. 8. Positions of the calibration rig estimated by the calibration software.

experiments: baseline $b = 35cm$, camera pitch angle $\alpha = 58deg$, scanning head mean angle $\beta = 90deg$. The calibration procedure yielded the following parameters: $b = 31.3cm$, camera pitch angle $\alpha = 53.3deg$, scanning head mean angle $\beta = 92.1deg$. A screenshot of this calibration can be seen in figure 9. This resemblance with the measured parameters confirms the general correctness of the calibration approach. Ideally it should be verified by using both sets of parameters to create 3D-scans of a known object and compare the results. This will be done in the future.

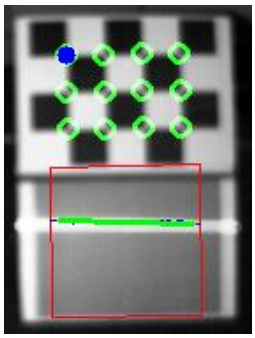

Fig. 9. Calibration rig image with recognized checkerboard-pattern at the top and extracted position of the laser-line at the bottom. The red rectangle represents the region which is searched for the laser line.

IV. Conclusion

A very interesting new approach has been presented for calibration of a triangulation-based laserscanner. The approach eliminates the necessity to measure any of the parameters of such a system manually, while at the same time keeping the calibration process simple enough to be applied in non-laboratory environments. Due to the improvement in parameter precision the overall precision of a 3d-laserscanning system is expected to be improved. Another advantage of this new approach is the possibility to specifically configure the system for a given task. A given set of baseline b, camera-pitch α and scanning head angle β results in an ideal scanning distance d, where the vertical field of view of the camera intersects the beams projected by the scanning head at minimum/maximum angles. Depending on the application different settings may be interesting, since only at the distance d does the 3D-laserscanner achieve its ideal scanning resolution. In existing systems some of these parameters may be fixed, while others can be varied. Due to the ease of the calibration process different settings may be tested and the best parameters for a given application selected.

Future work will be include thorough testing of the system in the underwater environment. An attempt will be made to include the seawater-refraction-compensation algorithm described in [13] to compensate for the non-colinearity error resulting from the different refractive indices.

Acknowledgment

The authors would like to thank all colleagues at the DFKI Bremen for their support and numerous positive feedback and ideas.

References

[1] Michael J. Chantler and J. Clark and M. Umasuthan, *Calibration and operation of an underwater laser triangulation sensor: the varying baseline problem*, Society of Photo-Optical Instrumentation Engineers, Opt.Eng Vol. 36(9) pages 2604-2611, September 1997.

[2] Chau-Chang Wang and Min-Shine Cheng, *Nonmetric Camera Calibration for Underwater Laser Scanning System*, IEEE Journal of Oceanic Engineering, Vol. 32, No. 2, pages 383-399, April 2007.

[3] F. Dalgleish and S. Tetlow and R. L. Allwood, *Seabed-relative navigation by hybrid structured lighting*, IEE Control Engineering Series, Vol. 69, pages 277-292, 2006.

[4] Y. Zheng and K. Yang and J. Rao and M. Xia, *A compact remote-controlled underwater lidar system*, Proceedings of the SPIE, Vol. 6451, pages 64511V, 2007.

[5] Simon Winkelbach and Sven Molkenstruck and Friedrich M. Wahl, *Low-Cost Laser Range Scanner and Fast Surface Registration Approach*, Lecture Notes in Computer Science, Vol. 4174, pages 718-728, Springer Berlin/Heidelberg, 2006

[6] Roderik Lindenbergh and Norbert Pfeifer and Tahir Rabbani, *Accuracy Analysis of the Leica HDS3000 and Feasability of Tunnel Deformation Monitoring*, ISPRS WG III/3, III/4, V/3 Workshop "Laser scanning 2005", Enschede, the Netherlands, September 12-14, 2005

[7] Dan Murfey, *2005 3D Laser Scanner Hardware Survey*, POB Point of Beginning, pages 72-77, January 2005

[8] L. Kou and D. Labrie and P. Chylek, *Refractive indices of water and ice in the 0.65-2.5 m spectral range*, Applied Optics, Vol. 32, pages 3531-3540, 1993.

[9] F. M. Sogandares and E. S. Fry, *Absorption spectrum (340-640nm) of pure water. I. Photothermal Measurements*, Applied Optics, Vol. 36, pages 8699-8709, 1997.

[10] Donna M. Kocak and Frank M. Caimi and Partha S. Das and Jeffery A. Karson, *A 3-D Laser Line Scanner for Outcrop Scale Studies of Seafloor Feature*, OCEANS '99 MTS/IEEE. Riding the Crest into the 21st Century, Vol. 3, pages 1105-1114, 1999.

[11] Sergio Ortiz and Jose Diaz-Caro and Rosario Pareja, *Radiometric modeling of a 3D imaging laser scanner*, Proceedings of the SPIE, Vol. 5987, pages 88-98, 2005.

[12] Z. Zhang, *A flexible new technique for camera calibration*, IEEE Transactions on Pattern Analysis and Machine Intelligence, Vol. 22(11), pages 1330-1334, 2000.

[13] R. Li and H. Li and W. Zou and R.G. Smith and T.A. Curran, *Quantative photogrammetric analysis of digital underwater video imagery*, IEEE Journal of Oceanic Engineering, Vol. 22, No. 2, pages 364-375, April 1997.